ACS APPLIED MATERIALS & INTERFACES

Letter

www.acsami.org

Perpendicular Exchange-Biased Magnetotransport at the Vertical Heterointerfaces in $La_{0.7}Sr_{0.3}MnO_3$:NiO Nanocomposites

Wenrui Zhang,[†] Leigang Li,[†] Ping Lu,[‡] Meng Fan,[§] Qing Su,[†] Fauzia Khatkhatay,[§] Aiping Chen,[⊥] Quanxi Jia,[⊥] Xinghang Zhang,[#] Judith L. MacManus-Driscoll,[∥] and Haiyan Wang*[,†,§]

[†]Department of Materials Science and Engineering, [§]Department of Electrical and Computer Engineering, and [#]Department of Mechanical Engineering, Texas A&M University, College Station, Texas 77843, United States

[‡]Sandia National Laboratories, Albuquerque, New Mexico 87185, United States

[⊥]Center for Integrated Nanotechnologies, MS K771, Los Alamos National Laboratory, Los Alamos, New Mexico 87545, United States

[∥]Department of Materials Science and Metallurgy, University of Cambridge, 27 Charles Babbage Road, Cambridge CB3 OFS, United Kingdom

Supporting Information

ABSTRACT: Heterointerfaces in manganite-based heterostructures in either layered or vertical geometry control their magnetotransport properties. Instead of using spin-polarized tunneling across the interface, a unique approach based on the magnetic exchange coupling along the vertical interface to control the magnetotransport properties has been demonstrated. By coupling ferromagnetic $La_{0.7}Sr_{0.3}MnO_3$ and antiferromagnetic NiO in an epitaxial vertically aligned nanocomposite (VAN) architecture, a dynamic and reversible switch of the resistivity between two distinct exchange biased states has been achieved. This study explores the use of vertical interfacial exchange coupling to tailor magnetotransport properties, and demonstrates their viability for spintronic applications.

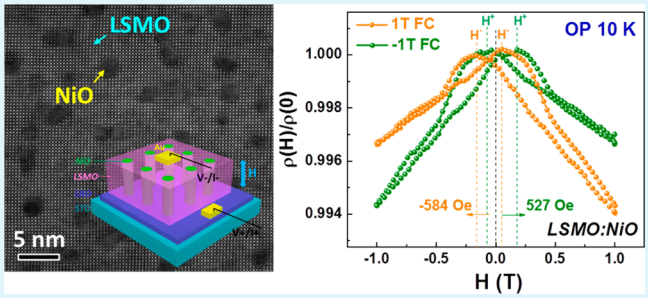

KEYWORDS: *vertically aligned nanocomposites (VAN), interface, magnetotransport, exchange bias, perpendicular anisotropy*

Heterointerfaces constructed in complex oxides add an extra degree of freedom for obtaining unexpected physical properties. Such heterointerfaces are typically achieved in a horizontal layered geometry such as bilayers, multilayers and superlattices.[1,2] Vertically oriented heterointerfaces in self-assembled two-phase vertically aligned nanocomposite (VAN) films have emerged very recently as another promising pathway for enhanced and tunable functionalities.[3−5] For example, the vertical strain coupling, because of the lattice mismatch between two component phases, could lead to enhanced physical properties and new functionalities which are difficult to achieve using the single phase constituents. Representative examples include sizable magnetoelectric coupling in both $BaTiO_3$:$CoFe_2O_4$[6] and $BiFeO_3$:$CoFe_2O_4$ films,[7] and increased Curie temperature in $BaTiO_3$:Sm_2O_3 films through nanocomposite-induced strain.[8] Besides, the increased spin scattering effect across the grain/phase boundaries has been employed to enhance the magnetotransport properties in $La_{0.7}Sr_{0.3}MnO_3$ (LSMO):ZnO nanocomposite films.[9,10]

The low-field magnetoresistance (LFMR) in manganite-based materials is one of most intriguing phenomena with promising applications for magnetic memory devices. The nanocomposite approach has been widely used to improve the LFMR performance by introducing secondary phases such as ZnO,[9,10] MgO,[11] CeO_2,[12] NiO,[13] and glass.[14] Despite different microstructures related to specific material systems, substrate lattice parameters, and orientations, the magnetotransport properties in VAN films are mostly investigated in the current-in-plane geometry (simplified as in-plane (IP) in the following section), where the current transports perpendicular to the vertical heterointerfaces. However, studies on electron transport along the vertical heterointerfaces (the current-perpendicular-to-plane geometry, simplified as out-of-plane (OP)), particularly the magnetotransport, are scarce. On the other hand, the exchange bias effect, i.e., originating from interfacial magnetic coupling and pinning effects at the ferromagnetic-antiferromagnetic (FM-AFM) heterointerfaces, has been exploited in commercial magnetic storage devices.[15,16] The strong interactions between the spin configuration and the electron transfer are expected to add another degree of control on the magnetotransport in the OP geometry. Here, we demonstrate perpendicular exchange biased magnetotransport using the strong magnetic exchange coupling at the vertical FM-AFM heterointerfaces. A LSMO:NiO (FM-AFM) VAN

Received: July 14, 2015
Accepted: September 23, 2015
Published: September 23, 2015

DOI: 10.1021/acsami.5b06314
ACS Appl. Mater. Interfaces 2015, 7, 21646−21651

system has been selected for this demonstration. Besides the anisotropic electron transport behavior, the magnetotransport property of the VAN films could be reversibly switched between two distinct exchange-biased states under an applied magnetic field through a field cooling procedure.

Figure 1a shows the typical $\theta-2\theta$ XRD scans of both LSMO:NiO VAN and pure LSMO films with the same

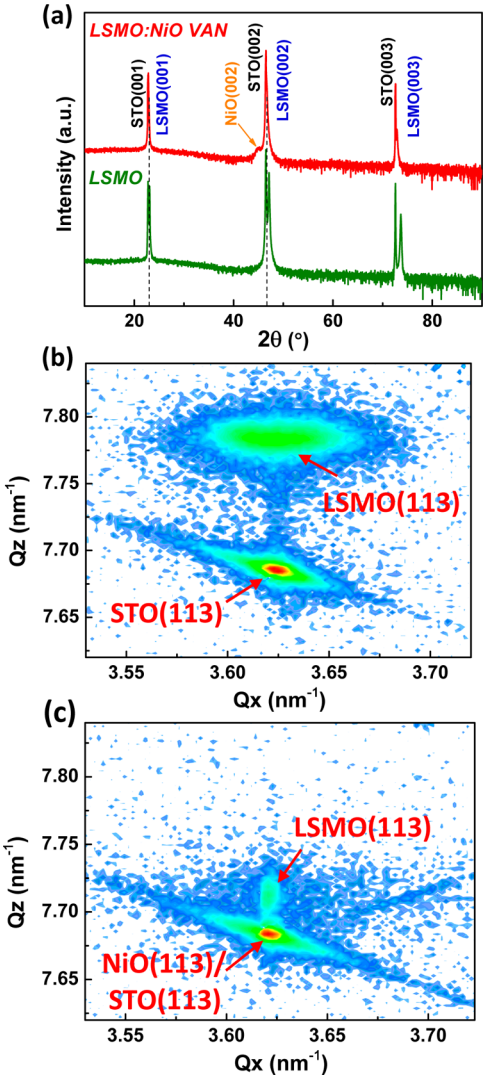

Figure 1. (a) $\theta-2\theta$ XRD scans of pure LSMO and LSMO:NiO VAN films. (b, c) Reciprocal space maps near (113) STO for (b) pure LSMO and (c) LSMO:NiO nanocomposite films on the STO (001) substrate.

thickness. It is obvious that only the LSMO (00*l*) and NiO (00*l*) peaks are present along with the $SrTiO_3$ (STO) (00*l*) peaks, indicating the highly textured OP film growth. Figure 1b, c shows the reciprocal space maps (RSM) near the substrate STO (113) peak of the pure LSMO and the LSMO:NiO films, respectively. The broad LSMO peak observed in the pure film indicates a systematic variation of lattice parameters as there is a gradual substrate-induced strain relaxation with increasing film thickness. In the VAN film, however, the LSMO (113) peak is shifted much closer to STO (113) peak with a much narrower lattice parameter variation as indicated by the sharper peak. A similar peak shift and narrower peak have also been observed in the RSM data near STO (002) for pure LSMO and LSMO:NiO films, respectively (see Figure S1), suggesting a vertical strain coupling between LSMO ($d_{LSMO\langle001\rangle}$ = 3.87 Å) and NiO ($d_{NiO\langle001\rangle}$4.17 Å). For the VAN films, the RSM peak shift of LSMO corresponds to an OP tensile strain of 0.53% (with respect to the pure film) and a more relaxed IP tensile strain of 0.08%.

Transmission electron microscopy (TEM) and scanning transmission electron microscopy (STEM) analyses in the high-angle annular dark-field (HAADF) mode were conducted to investigate the microstructure and phase distribution of the LSMO:NiO VAN films. Figure 2a shows the plan-view STEM image of a LSMO:NiO nanocomposite film. It is obvious that self-assembled NiO nanocolumns (in dark contrast) with an average diameter of 2 nm and an interspacing of 3.5 nm are uniformly distributed in the LSMO matrix (in bright contrast). The inset in the Figure 2a shows a high-resolution image of a single NiO nanopillar within the LSMO matrix, demonstrating very high epitaxial quality of these two phases and atomically sharp heterointerface between them. The energy-dispersive X-ray spectroscopy (EDS) mapping results demonstrate distinct phase separation between NiO and LSMO (Figure 2b). The self-assembled VAN structures can also be seen from their low magnification cross-sectional STEM image and the high-resolution TEM image (Figure 2c, d). The corresponding selected area electron diffraction (SAED) pattern in Figure 2e combined with the above XRD results confirms the orientation relationships between LSMO and NiO with the underlying STO substrate, i.e., $(001)_{LSMO} \parallel (001)_{NiO} \parallel (001)_{STO}$ (out-of-plane) and $[100]_{LSMO} \parallel [100]_{NiO} \parallel [100]_{STO}$ (in-plane).

Electrical transport measurements were carried out in both IP and OP configurations for pure LSMO and LSMO:NiO VAN films, as illustrated in the schematics in Figure 3a (OP, top left, and IP, bottom right). The external magnetic field was applied along the OP direction for magnetotransport measurements. A 15 nm-thick $SrRuO_3$ (SRO) bottom electrode was applied for OP measurements. Figure 3a shows the temperature dependent IP and OP normalized resistivity (R(T)) of the LSMO:NiO VAN film (ρ_{OP-VAN} and ρ_{IP-VAN}). A metal-to-insulator transition has been observed in ρ_{IP-VAN} with a transition temperature (T_{MI}) of ~248 K, which could be attributed to the strong suppression of double exchange interaction between the neighboring LSMO grains decoupled by NiO. On the other hand, a continuous decrease in ρ_{OP-VAN} has been observed within the test temperature range. This can be explained by the fact that the electron transport is mainly through the conducting LSMO channels along the OP direction. Because of the series connection between the upper films and the SRO, the possible contribution from SRO on the entire film resistivity has been carefully examined. It is also noted that the effect from SRO is minor with the incorporation of NiO in VAN films, as evidenced by the increase in ρ(10 K)/ρ(340 K) ratio from the bare SRO layer (15.8%) (see Figure S2) to those in series connected with pure LSMO (25.4%) and LSMO:NiO VAN films (62.2%). As a comparison, the $R(T)$ curves of the pure LSMO film were also presented. In Figure 3b, both $\rho_{IP-LSMO}$ and $\rho_{OP-LSMO}$ decrease monotonously with decreasing test temperature from 340 to 10 K and exhibit a metallic-like behavior below its Curie temperature (~350 K).[17]

The temperature-dependent MR data of both pure LSMO and LSMO:NiO VAN films show that ρ_{IP-VAN} has the largest MR value of −17.1% at ~227 K under the field of 1 T (see Figure S3), which could be explained by the largest spin-

DOI: 10.1021/acsami.5b06314
ACS Appl. Mater. Interfaces 2015, 7, 21646−21651

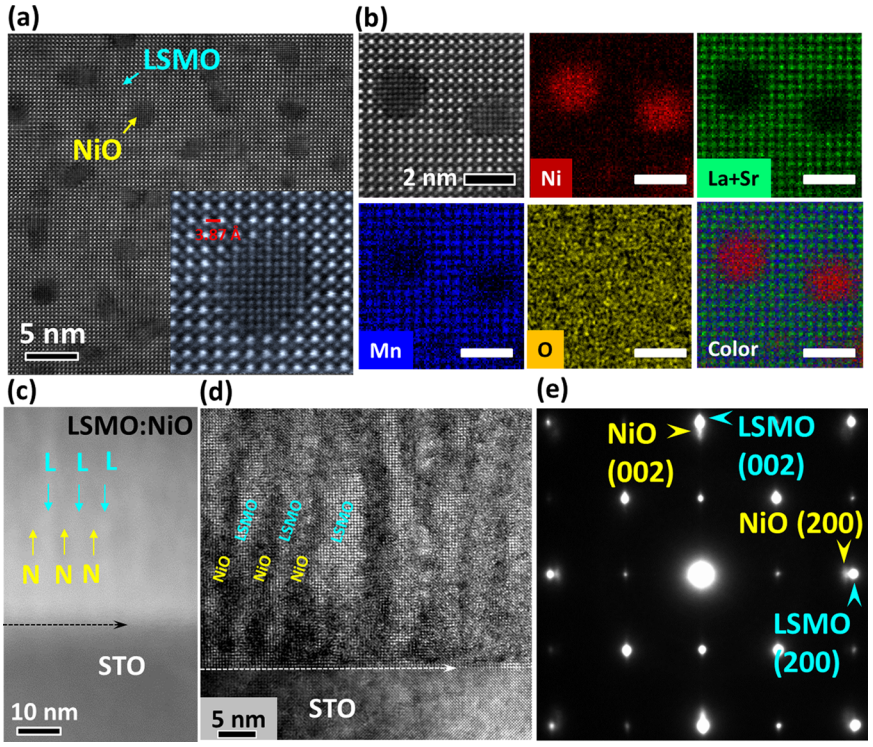

Figure 2. (a) Plan-view STEM image of the LSMO:NiO VAN film on the STO substrate. The inset shows a high-resolution image of a single NiO nanopillar embedded in the LSMO matrix. (b) EDS maps of Ni, La+Sr, Mn, O, and color map obtained from the area of the selected plan-view STEM image. (c) Cross-sectional STEM image and (d) high-resolution TEM image of the LSMO:NiO nanocomposite film showing periodically arranged nanopillars. (e) Corresponding SAED pattern of the cross-sectional TEM image in (d).

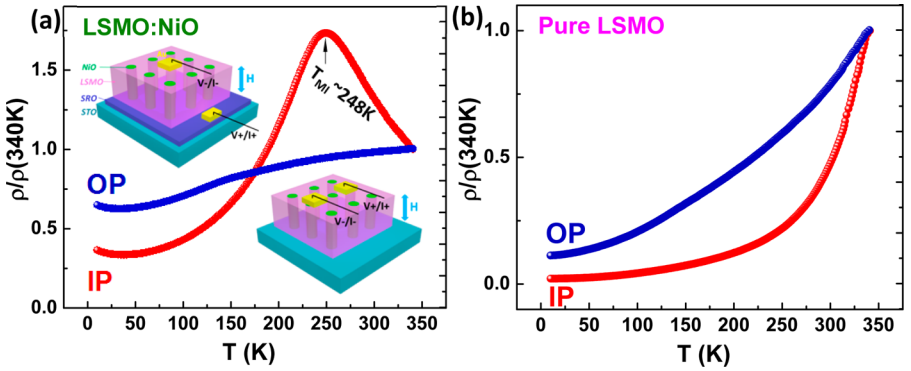

Figure 3. Temperature dependence of normalized OP and IP zero-field resistivity of (a) LSMO:NiO VAN and (b) pure LSMO films. Insets in (a) show the schematic drawings of out-of-plane (OP, top left) and in-plane (IP, bottom right) resistivity measurements, respectively. The magnetic field for magnetotransport measurements is applied perpendicular to the film surface.

dependent scattering and tunneling effects obtained in the IP configuration of the nanocomposite film.[18] More importantly, the focus of this study is to investigate the effect of the magnetic exchange coupling at the vertical heterointerfaces on the dynamic tunability of the magnetotransport property. Such a dynamic tuning effect has not yet been demonstrated in epitaxial VAN architectures and could provide an alternative way for magnetotransport control. Figure 4a shows the normalized ρ_{OP-VAN} versus the magnetic field (R(H)) measured at 10 K after field cooling (FC) under a magnetic field of 1 T and −1 T. $\rho(H)$ and $\rho(0)$ represent the resistivity with and without a magnetic field, respectively. It is interesting to observe that the R(H) curves shift toward either the negative or positive field with a pronounced bias field of −584 or 527 Oe, respectively depending on the cooling field direction. The asymmetric shape of R(H) curves is ascribed to the interfacial FM-AFM exchange coupling, which induces a unidirectional anisotropy (K_U) in the FM phase and influences its magnetotransport.[19] When the exchange coupling disappears under a zero field cooling, K_U vanishes and thus led to a more symmetric $R(H)$ curve (see Figure S4). To confirm the unique role of vertical exchange coupling in controlling the magnetotransport properties, the field-cooled R(H) data of ρ_{IP-VAN} (Figure 4b) and $\rho_{OP-LSMO}$ (see Figure S5a) were carefully examined, and no shift behavior has been observed.

The perpendicular exchange bias effect at LSMO:NiO vertical interfaces was further investigated by the magnetic hysteresis loops (M(H)) of the LSMO:NiO nanocomposite film measured at different temperatures. As shown in Figure 4c, after 1 T FC to 10 K, the M(H) curve of the LSMO:NiO film

DOI: 10.1021/acsami.5b06314
ACS Appl. Mater. Interfaces 2015, 7, 21646−21651

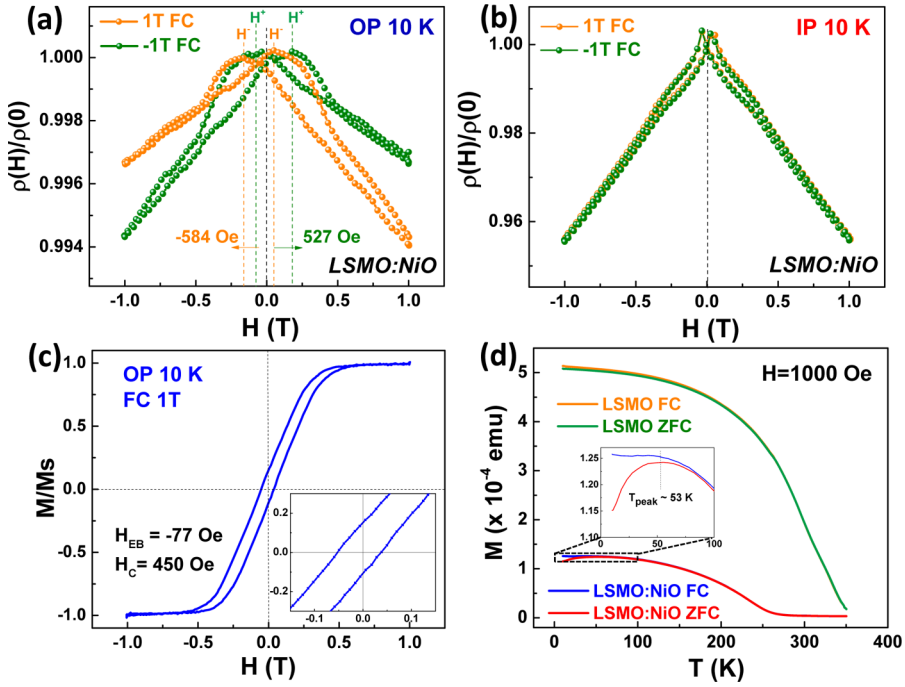

Figure 4. (a, b) Magnetic field dependence of normalized (a) ρ_{OP} and (b) ρ_{IP} of the LSMO:NiO VAN film after FC to 10 K in a 1 T and −1 T field. (c) Magnetic hysteresis curves of the LSMO:NiO film with the same FC procedure. The inset is the enlarged part of the bias shift. (d) Temperature dependence of ZFC and FC magnetization of pure LSMO and LSMO:NiO films measured with a IP magnetic field of 1000 Oe. The inset shows the enlarged part of the bifurcation behavior between ZFC and FC curves.

exhibits a horizontal shift with an exchange bias field (H_{EB}) of −77 Oe and a coercive field (H_c) of 450 Oe. In comparison, the FC data of the LSMO film shows no bias shift and a smaller H_c of 396 Oe due to the lack of exchange coupling (see Figure S5b). It is noted that the H_{EB} and H_c obtained from the M(H) curves are much smaller than those from the R(H) results. The discrepancy can be understood by the difference between these two measurement techniques. The bias fields measured from R(H) tests are determined by the average pinning field of the entire FM-AFM interfaces, while the values from M(H) curves are dominated by the weakest site for the occurrence of nucleation during the magnetization reversal.[20,21] Hence the M(H) technique measures the lowest limit of the actual H_{EB} associated with the weakest pinned region, and thus gives much smaller values than those from R(H) tests. In the material systems with uniform exchange coupling at the interface, the H_{EB} values measured from M(H) and R(H) tests agree with each other, as observed in FeMn/NiFe exchange biased spin valves[22] and high-quality CoO/Co and CoO/Fe bilayers.[23] On the other hand, the discrepancy of H_{EB} becomes significant in the presence of irreversible AFM domain formation and rearranged spin coupling, which strongly relates to the interface structure and geometry. Similar effects have also been observed in previous studies of exchange biased Co/CoO bilayers[24] and antidote arrays[20,25] probed with magnetization hysteresis and anisotropic MR techniques. In LSMO:NiO VAN films, the self-assembled high-density vertical interfaces give rise to larger interfacial spin fluctuations and thus leads to the observed discrepancy effect.

Figure 4d presents the zero-field-ooling (ZFC) and FC data of magnetization as a function of temperature ($M(T)$) measured with an in-plane magnetic field of 1000 Oe. First, it is noticed that the measured T_c (~234 K, defined as the temperature where the dM/dT reaches the minimum value) is consistent with the T_{MI} measured in Figure 3a (i.e., 248 K). The bifurcation between the ZFC and FC M(T) curves at T_{irr} (~75 K) and a peak observed in ZFC MT data at T_{peak} (~53 K) indicates the existence of spin-disordered states in the VAN film, which is not seen in the pure LSMO film. This could result from the competing magnetic orders and spin frustration at LSMO-NiO heterointerfaces, as seen in other LSMO-based heterostructures.[18,26] As the temperature increases, the magnetic exchange coupling strength between LSMO and NiO is significantly weakened with a rapid decay of the FM ordering in LSMO. As the measurement temperature increases to 150 K, the $R(H)$ curve after 1 T cooling to 150 K presents no shift to either direction (see Figure S6a), and the H_{EB} from the $M(H)$ measurement decreases to 0 Oe accompanied by a decrease of the coercive field (see Figure S6b), suggesting a full relaxation of the exchange coupling between LSMO and NiO.

The above experimental results demonstrate the unique role played by perpendicular exchange coupling at vertical heterointerfaces in LSMO:NiO VAN films on the tuning of the OP magnetotransport properties. The strong dependence of the OP electron transport on the interfacial exchange coupling indicates a different transport-controlled mechanism compared to those reported in bilayer/multilayers, polycrystalline nanocomposite and bulk materials. In conventional layered magnetic tunneling junctions (MTJs) or VAN structures for in-plane transport, the spin-polarized tunneling and spin filtering effects have been typically used to enhance the magnetotransport property.[27−29] On the other hand, for the OP transport of the VAN films, the spin-polarized tunneling effect becomes minor because the tunneling barrier thickness (equivalent to the film thickness) is extremely high and electrons are mainly transported through the conducting channels. Instead, the interfacial exchange coupling at the vertical interface introduces anisotropic constraints on the FM spin rotation during external

DOI: 10.1021/acsami.5b06314
ACS Appl. Mater. Interfaces 2015, 7, 21646−21651

perpendicular field switching, and thus influences the magnetotransport properties. More importantly, by tuning the vertical interface density in the VAN structure, one can control the overall exchange coupling strength and resultant magnetotransport properties. This has been evidenced by comparing the results of LSMO:NiO VAN films with different nanopillar sizes and interspacings. As shown in Figure S7, when the deposition frequency was reduced to 1 Hz, the LSMO:NiO VAN film with a larger nanopillar size (~3.3 nm) and interspacing (~5.7 nm) was obtained. This resulted in reduced pillar density and vertical interface density. As a result, the $R(H)$ curves showed a much smaller shift (~50 Oe) under the same FC procedure.

In summary, self-assembled LSMO:NiO vertically aligned nanocomposite films were grown using pulsed laser deposition with a uniform morphology of highly ordered, ultrafine NiO nanopillars embedded in the LSMO matrix. The anisotropic electron transport properties in both the current-in-plane (IP) and current-out-of-plane (OP) geometries were investigated. The vertical LSMO-NiO heterointerfaces in the nanocomposite films demonstrated pronounced magnetic exchange coupling at low temperatures, as indicated by the observed exchange bias effect. More interestingly, such a vertical interface coupling enables a dynamic and reversible control of magnetotransport properties. The work demonstrates that exchange coupling of vertical FM-AFM heterointerfaces represents an alternative approach to manipulating magnetotransport properties in epitaxial oxide nanocomposite films.

EXPERIMENTAL SECTION

Pure LSMO films and LSMO:NiO (with a molar ratio of 3:2) nanocomposite films with a thickness of 70−100 nm were grown on single-crystal $SrTiO_3$ (001) substrates at 750 °C in 200 mTorr of oxygen using pulsed laser deposition with a KrF laser (Lamda Physik, λ = 248 nm) at a repetition rate of 10 Hz. The laser energy density is 2.2 J/cm^2. After the depositions, the samples were cooled down in an oxygen pressure of 200 Torr at a cooling rate of 5 °C/min. The epitaxial quality and microstructure of all samples were investigated with high-resolution XRD (PANalytical Empyrean diffractometer) using Cu−K_α radiation and TEM (FEI Tecnai G^2 F20). For high-resolution STEM and EDS mapping, a FEI Titan G2 800−200 STEM with as a Cs probe corrector and ChemiSTEM technology (X-FEG and SuperX EDS with four windowless silicon drift detectors) operated at 200 kV was used. Au electrodes were deposited by sputtering on top of films for electrical property measurements. The sample resistivity was measured in a Physical Properties Measurement System (PPMS, Quantum Design). For the field-cooling (FC) and zero field cooling (ZFC) measurements, the samples were cooled down from 300 K to target temperatures under magnetic fields of 1 and 0 T, respectively. The substrate signals have been subtracted for all measured samples.

ASSOCIATED CONTENT

Supporting Information

The Supporting Information is available free of charge on the ACS Publications website at DOI: 10.1021/acsami.5b06314.

Reciprocal space mapping results near the (002) STO peak of pure LSMO and LSMO:NiO VAN films, temperature dependence of resistivity of bare SRO layer, pure LSMO and LSMO:NiO VAN films under different magnetic fields, magnetic field-dependence of resistivity, and magnetic hysteresis loop of pure LSMO and LSMO:NiO VAN films measured at different temperatures, plan-view TEM image, electron diffraction data, temperature-dependent and magnetic-field-dependent resistivity of LSMO:NiO VAN film deposited by 1 Hz (PDF)

AUTHOR INFORMATION

Corresponding Author

*E-mail: wangh@ece.tamu.edu.

Notes

The authors declare no competing financial interest.

ACKNOWLEDGMENTS

This work was supported by the U.S. National Science Foundation (Ceramic Program, DMR-1401266 (VAN design and growth) and DMR-0846504 (high-resolution STEM analysis)). Sandia National Laboratories is a multiprogram laboratory managed and operated by Sandia Corporation, a wholly owned subsidiary of Lockheed Martin Corporation, for the U.S. Department of Energy's National Nuclear Security Administration under contract DE-AC04-94AL85000. J.L.M.-D. acknowledges support from the Engineering and Physical Sciences Research Council of the UK, (EP/P50385X/1), and the European Research Council (ERC-2009-AdG 247276 NOVOX). The work at Los Alamos was partially supported by the Laboratory Directed Research and Development Program and was performed, in part, at the Center for Integrated Nanotechnologies, an Office of Science User Facility operated for the U.S. Department of Energy (DOE) Office of Science.

REFERENCES

(1) Hwang, H. Y.; Iwasa, Y.; Kawasaki, M.; Keimer, B.; Nagaosa, N.; Tokura, Y. Emergent Phenomena at Oxide Interfaces. *Nat. Mater.* **2012**, *11*, 103−113.

(2) Yu, P.; Chu, Y.-H.; Ramesh, R. Oxide Interfaces: Pathways to Novel Phenomena. *Mater. Today* **2012**, *15*, 320−327.

(3) MacManus-Driscoll, J. L.; Zerrer, P.; Wang, H.; Yang, H.; Yoon, J.; Fouchet, A.; Yu, R.; Blamire, M. G.; Jia, Q. X. Strain Control and Spontaneous Phase Ordering In Vertical Nanocomposite Heteroepitaxial Thin Films. *Nat. Mater.* **2008**, *7*, 314−320.

(4) Zhang, W.; Chen, A.; Bi, Z.; Jia, Q. X.; MacManus-Driscoll, J. L.; Wang, H. Interfacial Coupling in Heteroepitaxial Vertically Aligned Nanocomposite Thin Films: From Lateral to Vertical Control. *Curr. Opin. Solid State Mater. Sci.* **2014**, *18*, 6−18.

(5) Liu, H.-J.; Liang, W.-I.; Chu, Y.-H.; Zheng, H.; Ramesh, R. Self-assembled Vertical Heteroepitaxial Nanostructures: From Growth to Functionalities. *MRS Commun.* **2014**, *4*, 31−44.

(6) Zheng, H.; Wang, J.; Lofland, S. E.; Ma, Z.; Mohaddes-Ardabili, L.; Zhao, T.; Salamanca-Riba, L.; Shinde, S. R.; Ogale, S. B.; Bai, F.; Viehland, D.; Jia, Y.; Schlom, D. G.; Wuttig, M.; Roytburd, A.; Ramesh, R. Multiferroic $BaTiO_3$-$CoFe_2O_4$ Nanostructures. *Science* **2004**, *303*, 661−663.

(7) Zavaliche, F.; Zheng, H.; Mohaddes-Ardabili, L.; Yang, S. Y.; Zhan, Q.; Shafer, P.; Reilly, E.; Chopdekar, R.; Jia, Y.; Wright, P.; Schlom, D. G.; Suzuki, Y.; Ramesh, R. Electric Field-Induced Magnetization Switching in Epitaxial Columnar Nanostructures. *Nano Lett.* **2005**, *5*, 1793−1796.

(8) Harrington, S.; Zhai, J.; Denev, S.; Gopalan, V.; Wang, H.; Bi, Z.; Redfern, S. A. T.; Baek, S.-H.; Bark, C. W.; Eom, C.-B.; Jia, Q. X.; Vickers, M. E.; MacManus-Driscoll, J. L. Thick Lead-free Ferroelectric Films with High Curie Temperatures through Nanocomposite-induced Strain. *Nat. Nanotechnol.* **2011**, *6*, 491−495.

(9) Zhang, W.; Chen, A.; Khatkhatay, F.; Tsai, C.-F.; Su, Q.; Jiao, L.; Zhang, X.; Wang, H. Integration of Self-Assembled Vertically Aligned Nanocomposite $(La_{0.7}Sr_{0.3}MnO_3)_{1-x}$:$(ZnO)_x$ Thin Films on Silicon Substrates. *ACS Appl. Mater. Interfaces* **2013**, *5*, 3995−3999.

DOI: 10.1021/acsami.5b06314
ACS Appl. Mater. Interfaces 2015, 7, 21646−21651

(10) Chen, A.; Zhang, W.; Khatkhatay, F.; Su, Q.; Tsai, C.-F.; Chen, L.; Jia, Q. X.; MacManus-Driscoll, J. L.; Wang, H. Magnetotransport Properties of Quasi-one-dimensionally Channeled Vertically Aligned Heteroepitaxial Nanomazes. *Appl. Phys. Lett.* **2013**, *102*, 093114.
(11) Lebedev, O. I.; Verbeeck, J.; Van Tendeloo, G.; Shapoval, O.; Belenchuk, A.; Moshnyaga, V.; Damashcke, B.; Samwer, K. Structural Phase Transitions and Stress Accommodation in $(La_{0.67}Ca_{0.33}MnO_3)_{1-x}$:$(MgO)_x$ Composite Films. *Phys. Rev. B: Condens. Matter Mater. Phys.* **2002**, *66*, 104421.
(12) Chen, A.; Bi, Z.; Hazariwala, H.; Zhang, X.; Su, Q.; Chen, L.; Jia, Q. X.; MacManus-Driscoll, J. L.; Wang, H. Microstructure, Magnetic, and Low-field Magnetotransport Properties of Self-assembled $(La_{0.7}Sr_{0.3}MnO_3)_{0.5}$:$(CeO_2)_{0.5}$ Vertically Aligned Nanocomposite Thin Films. *Nanotechnology* **2011**, *22*, 315712.
(13) Ning, X.; Wang, Z.; Zhang, Z. Large, Temperature-Tunable Low-Field Magnetoresistance in $La_{0.7}Sr_{0.3}MnO_3$ Nanocomposite Films Modulated by Microstructures. *Adv. Funct. Mater.* **2014**, *24*, 5393−5401.
(14) Gupta, S.; Ranjit, R.; Mitra, C.; Raychaudhuri, P.; Pinto, R. Enhanced Room-Temperature Magnetoresistance in $La_{0.7}Sr_{0.3}MnO_3$-glass Composites. *Appl. Phys. Lett.* **2001**, *78*, 362−364.
(15) Nogués, J.; Schuller, I. K. Exchange Bias. *J. Magn. Magn. Mater.* **1999**, *192*, 203−232.
(16) Wu, S. M.; Cybart, S. A.; Yu, P.; Rossell, M. D.; Zhang, J. X.; Ramesh, R.; Dynes, R. C. Reversible Electric Control of Exchange Bias in A Multiferroic Field-effect Device. *Nat. Mater.* **2010**, *9*, 756−761.
(17) Tsui, F.; Smoak, M. C.; Nath, T. K.; Eom, C. B. Strain-dependent Magnetic Phase Diagram of Epitaxial $La_{0.67}Sr_{0.33}MnO_3$ Thin Films. *Appl. Phys. Lett.* **2000**, *76*, 2421−2423.
(18) Chen, A.; Bi, Z.; Tsai, C.-F.; Lee, J.; Su, Q.; Zhang, X.; Jia, Q. X.; MacManus-Driscoll, J. L.; Wang, H. Tunable Low-Field Magnetoresistance in $(La_{0.7}Sr_{0.3}MnO_3)_{0.5}$:$(ZnO)_{0.5}$ Self-Assembled Vertically Aligned Nanocomposite Thin Films. *Adv. Funct. Mater.* **2011**, *21*, 2423−2429.
(19) Camarero, J.; Sort, J.; Hoffmann, A.; García-Martín, J. M.; Dieny, B.; Miranda, R.; Nogués, J. Origin of the Asymmetric Magnetization Reversal Behavior in Exchange-Biased Systems: Competing Anisotropies. *Phys. Rev. Lett.* **2005**, *95*, 057204.
(20) Tripathy, D.; Adeyeye, A. O. Probing the Exchange Bias in Co/CoO Nanoscale Antidot Arrays Using Anisotropic Magnetoresistance. *Phys. Rev. B: Condens. Matter Mater. Phys.* **2009**, *79*, 064413.
(21) Gredig, T.; Krivorotov, I. N.; Dahlberg, E. D. Temperature Dependence of Magnetization Reversal and Angular Torque in Co/CoO. *Phys. Rev. B: Condens. Matter Mater. Phys.* **2006**, *74*, 094431.
(22) Paul, A.; Buchmeier, M.; Bürgler, D. E.; Grünberg, P. Rotating-field Magnetoresistance of Exchange-biased Spin Valves. *J. Appl. Phys.* **2005**, *97*, 023910.
(23) Gruyters, M. Anisotropic Magnetoresistance in CoO/Co and CoO/Fe Bilayers in the Biased and Unbiased State. *J. Appl. Phys.* **2004**, *95*, 2587−2592.
(24) Gredig, T.; Krivorotov, I. N.; Dahlberg, E. D. Magnetization Reversal in Exchange Biased Co/CoO Probed with Anisotropic Magnetoresistance. *J. Appl. Phys.* **2002**, *91*, 7760−7762.
(25) Tripathy, D.; Vavassori, P.; Porro, J. M.; Adeyeye, A. O.; Singh, N. Magnetization Reversal and Anisotropic Magnetoresistance Behavior in Bicomponent Antidot Nanostructures. *Appl. Phys. Lett.* **2010**, *97*, 042512.
(26) Ding, J. F.; Lebedev, O. I.; Turner, S.; Tian, Y. F.; Hu, W. J.; Seo, J. W.; Panagopoulos, C.; Prellier, W.; Van Tendeloo, G.; Wu, T. Interfacial Spin Glass State and Exchange Bias in Manganite Bilayers with Competing Magnetic Orders. *Phys. Rev. B: Condens. Matter Mater. Phys.* **2013**, *87*, 054428.
(27) Lu, Y.; Li, X. W.; Gong, G. Q.; Xiao, G.; Gupta, A.; Lecoeur, P.; Sun, J. Z.; Wang, Y. Y.; Dravid, V. P. Large Magnetotunneling Effect at Low Magnetic Fields in Micrometer-scale Epitaxial $La_{0.67}Sr_{0.33}MnO_3$ Tunnel Junctions. *Phys. Rev. B: Condens. Matter Mater. Phys.* **1996**, *54*, R8357−R8360.
(28) Prasad, B.; Egilmez, M.; Schoofs, F.; Fix, T.; Vickers, M. E.; Zhang, W.; Jian, J.; Wang, H.; Blamire, M. G. Nanopillar Spin Filter Tunnel Junctions with Manganite Barriers. *Nano Lett.* **2014**, *14*, 2789−2793.
(29) Chen, A.; Weigand, M.; Bi, Z.; Zhang, W.; Lu, X.; Dowden, P.; MacManus-Driscoll, J. L.; Wang, H.; Jia, Q. X. Evolution of Microstructure, Strain and Physical Properties in Oxide Nanocomposite Films. *Sci. Rep.* **2014**, *4*, 5426.

DOI: 10.1021/acsami.5b06314
ACS Appl. Mater. Interfaces 2015, 7, 21646−21651